ROYAL SOCIETY
OF CHEMISTRY

PAPER

Controlled assembly of cobalt embedded N-doped graphene nanosheets (Co@NGr) by pyrolysis of a mixed ligand Co(II) MOF as a sacrificial template for high-performance electrocatalysts†

Gopala Ram Bhadu, [ID] *[a] Bhavesh Parmar, [ID][a] Parth Patel, [ID][bc]
Jayesh C. Chaudhari [ID][a] and Eringathodi Suresh [ID] *[ad]

The development of high-efficiency and durable bifunctional electrocatalysts is an important and challenging topic in the area of energy storage/conversion. Herein, we prepared metallic cobalt nanoparticle decorated N-doped graphitic sheets (Co@NGr) by adopting facile pyrolysis of a mixed ligand cobalt-based MOF (CoMOF-2) as a sacrificial template displaying good OER and HER activity. The catalytic material harvested at three different pyrolytic temperatures was characterized by various analytical methods such as PXRD, SEM, TEM, Raman, and XPS analyses. The catalytic activity of the obtained hybrid composite materials towards oxygen evolution reaction (OER) and hydrogen evolution reaction (HER) was studied. Co@NGr-900 was found to be an efficient bifunctional electrocatalyst and 10 mA cm^{-2} current density was afforded at an overpotential of 390 mV for OER and 340 mV for HER respectively. This study provides insight for the development of cost-effective nonprecious element-based electrocatalysts for water splitting which has relevance in energy storage and conversion. Catalytic performance is governed by the synergistic compositional effect of metallic cobalt/nitrogen-doping in the graphitic carbon increasing the electrical conductivity/active sites of the composite material.

Introduction

Global energy demand continues to increase, mainly due to modern living, industrialization, emerging economies and rapid depletion of conventional fossil fuels. Fossil fuels as an energy source have a tremendous impact on greenhouse gas emissions along with climate change causing an adverse effect on the environment and a new alternative clean energy source is the requisite for the benefit of society. Research activities for the development of viable alternative green energy are in the limelight due to the rapid depletion of non-renewable energy sources. Energy supply of the future is based on renewable sources by tapping sustainable energy resources from solar, wind and water from nature.[1–4] Development of sustainable electrochemical energy technologies comprises converting chemical energy to electrical energy by fuel cells and utilizing clean and efficient hydrogen sources from water splitting as the energy carrier.[5,6] Electrochemical water splitting for the production of clean 'H$_2$' as a potential energy source is one of the most promising approaches in the transition towards sustainable energy resources. Slothful kinetics and high input potential requirement for the OER/HER during water splitting process hinder the overall efficiency and practical applications of this segment. Electrocatalytic water splitting in presence of an efficient catalyst provides a sustainable approach to generate clean energy through hydrogen evolution reaction (HER) and oxygen evolution reaction (OER).[7,8] Especially the OER has attracted research attention due to its wide range of application to energy conversion and storage technologies.[9,10] RuO$_2$ and IrO$_2$ are generally regarded as benchmark electrocatalysts because of their high electrocatalytic performance in the acidic as well as the alkaline solution towards OER.[11,12] Although, both state-of-the-art catalyst (RuO$_2$/IrO$_2$) are made of precious metals with low abundance/high cost and due to dissolution and easy oxidation to higher valance state impede their practical utility for large-scale OER catalyst.[13,14] Accordingly, to make water splitting process practically viable, substantial research effort has been devoted for the development of economical, more efficient and cost-effective electrocatalyst materials essential for

[a]Analytical and Environmental Science Division and Centralized Instrument Facility, CSIR – Central Salt and Marine Chemicals Research Institute, G. B. Marg, Bhavnagar-364 002, Gujarat, India. E-mail: grbhadu@csmcri.res.in; esuresh@csmcri.res.in; sureshe123@rediffmail.com

[b]Inorganic Materials and Catalysis Division, CSIR – Central Salt and Marine Chemicals Research Institute, G. B. Marg, Bhavnagar-364 002, Gujarat, India

[c]Charotar University of Science & Technology, Changa-388 421, Anand, Gujarat, India

[d]Academy of Scientific and Innovative Research (AcSIR), Ghaziabad-201 002, India

the real implementation of fuel cells, regenerative batteries, and electrolyzer systems.

Research focuses on alternative and affordable transition metal based OER electrocatalysts has gained much attention in the past decade. Thus, transition metal-based materials, which include transition metal oxides, hydroxides, chalcogenides, organometallic compounds, *etc.* has grown and captured eminence as OER electrocatalysts.[15–20] Despite significant progress, insufficient activity, stability as well as poor mass transport properties are the major bottlenecks associated with the development of new electrocatalytic material. Metal–organic frameworks (MOFs), a class of hybrid materials possessing tunable surface functional groups, good porosity/surface area, compositional versatility and homogeneous distribution of metal atoms stimulated remarkable interests in a variety of research fields.[21–27] In spite of the above mentioned attributes, due to the poor electron conducting properties, low diffusion of reactants through MOF porosity, saturation of coordination geometry of metal centers and low reactivity of metal centers, most MOFs being not efficient as the electrode materials or electrocatalysts.[28] Hence, research activities have been focused on the pyrolysis of MOF as sacrificial template to produce functional nanostructured carbon materials towards electrocatalytic application. In fact, nanostructured carbon and composite materials comprising metal–nitrogen–carbon (M–N–C) systems with earth abundant transition metals derived from MOFs revealed excellent activities as low cost electrocatalyst.[29–34] Among M–N–Cs, Co embedded nonprecious transition metal with nitrogen co-doped carbon composite has been demonstrated as an efficient costeffective electrocatalyst due to the concomitant inherent assets such as porous nature of the graphitic carbon and conducting property of metal and nitrogen present in the system.[35–37] General strategy adopted for synthesis of M–N–C based electrocatalytic composites for ORR/OER comprises pyrolysis of the desired metal salt along with nitrogen/carbon rich precursors resulting low-density active sites with anomalies in structural uniformity and porosity. MOFs composed of metal nodes and appropriate N/C-contained organic linkers are an ideal candidate as a sacrificial template to achieve uniform structure, with porosity and available active sites for the rational design of M–N–C OER/HER catalysts by carbonization.

Motivated by the inherent electrical properties of the cobalt metal, porous nature of graphitic carbon and the excellent OER properties of the Co–N–C nanostructured materials from previous studies, development of a smart cobalt embedded carbon composite is an effective approach to promote the electrochemical application.[38–45] The active metal nanoparticles and N-doped graphitic carbon shell in composite materials can concomitantly improve the OER and HER activity.[46,47] Based on these background, we have chosen rationally designed Co(II) based mixed ligand 3D MOF (CoMOF-2) composed of N-donor and aromatic dicarboxylate ligands for the fabrication of Co–N–C based nanostructured material *via* high temperature pyrolysis. Bulk phase pure CoMOF-2 was prepared by conventional reflux method involving metal salt/ligand precursors in appropriate stoichiometry reported by us earlier.[48] Pyrolysis of

CoMOF-2 has been performed at three different temperatures (700/800/900 °C) to optimize the conditions and evaluated the progressive transformation of the material to develop Co–N–C based nanostructured material and assessed their electrocatalytic performance. Decomposition of CoMOF-2 by the carbonization at 900 °C under inert condition led to the formation of uniformly distributed cobalt encased N-doped graphene nanosheets (Co@NGr) anticipating excellent electrochemical performance. The composite carbon nanomaterial Co@NGr obtained by carbonization showed good OER and HER performance comparable with the benchmark noble electrocatalyst. Among the carbonized materials Co@NGr-900 showed good stability and excellent electrocatalytic performance toward OER and HER with an overpotential of 390 mV and 340 mV respectively under standard condition. MOF-derived hybrid nanocomposite Co@NGr-900 also sustained stability, R_{ct} as well as an electroactive surface area with excellent electrochemical activity. The high electrocatalytic performance of Co@NGr-900 can be ascribed to the presence of metallic Co nanoparticle, N-doping and porosity of carbon matrix. This work provides a viable approach for designing cobalt embedded N-doped graphene nanosheets (Co@NGr) as highly efficient electrocatalyst towards electrochemical water splitting, maybe useful in fabricating electrochemical energy storage and conversion.

Results and discussion

Material characterization

Synthesis of cobalt doped N-encased carbon nanocomposite embraces two steps. The first step consists of synthesis of the phase pure 3D mixed ligand CoMOF-2 composed of aromatic dicarboxylic acid (BDC = 1,4-benzenedicarboxylate) and acylamide decorated N-donor linker (L = (*E*)-*N*′-(pyridin-4-ylmethylene)isonicotinohydrazide). Pyrolysis of CoMOF-2 at three different temperatures 700, 800, 900 °C under N_2 atmosphere is the second step and the Co–N–C material attained has been labelled as Co@NGr-700, Co@NGr-800 and Co@NGr-900 respectively. Experimental details of the carbonization process are provided in the ESI.† It is worth mentioning here that bulk synthesis of CoMOF-2 with good phase purity has been accomplished by room temperature stirring of the precursors and the PXRD data is in good agreement with the simulated SXRD as per our previous report (Fig. S1†).[48] The bulk material has been characterized well with other physico-chemical methods also and the SXRD analysis of CoMOF-2 exposed that 2D $[M_2(BDC)_2]_n$ sheets constituted by the dimeric Co(II)-terephthalate clusters are doubly pillared by the Schiff base linker L generating the porous 3D framework (Fig. S2 and S3†). Anticipating the nanostructured carbon material with metal doping, pyrolysis of CoMOF-2 has been implemented at different temperatures, where the dicarboxylate/pyridine-based N-donor ligand with acylamide functional group can act as carbon/nitrogen source along with the uniformly distributed metallic cobalt. Characterization of the pyrolytic products collected under different annealing temperatures has been executed by various analytical methods (SEM/TEM analysis, PXRD, XPS, Raman and surface area analysis) to confirm the systematic

assembly of Co@NGr nanocomposite. Structural and morphological changes of the annealed CoMOF-2 material and the progressive evolution of the Co@NGr have been monitored and analyzed by microscopic techniques (TEM and FE-SEM). As depicted in SEM/TEM images, upon annealing at 700 °C (Co@NGr-700) in N_2 atmosphere, decomposition and gasification of CoMOF-2 3D framework commence with the controlled formation of graphitic carbon and precipitation of metallic cobalt retaining part of CoMOF-2 as unburned. The escape of the gases produced during the pyrolysis resulted in a rough surface that is composed of randomly agglomerated small particles with sizes ranging from several nanometers, yielding interconnected meso- and microporous ensembles as depicted in Fig. 1a and d.

SEM/TEM image of CoMOF-2 heat treated at 800 °C (Co@NGr-800) revealed the clusters of nanoparticles are agglomerated and inter-connected one another by coalescence, generating spherical morphology possessing highly porous closely distributed voids with rough surface entailing the formation of added carbonaceous matrix still retaining some intact CoMOF-2 (Fig. 1b and e). Fusion and expansion of the graphitic carbon matrix with complete transformation of the CoMOF-2 become apparent at 900 °C (Co@NGr-900) inducing the realization of hetero-atom doped carbon shell with homogeneously dispersed Co nanoparticle generating the anticipated product Co@NGr nanomaterial as depicted in Fig. 1c and f. Elemental analysis shown in Fig. 1g–k revealed the material is composed of Co, C, N, O supporting formation of Co@NGr-900. Co@NGr nanostructured material was further characterized by HR-TEM microscopic technique. The morphological changes including entrapment of metallic Co-nanoparticle in the carbon matrix upon temperature variation of the annealed products are clearly visible in the HR-TEM image (Fig. 2 and S4–S6†). Interestingly, with an increase in annealing temperature, the embedded cobalt nanoparticle retains almost similar average size and the complete decomposition of the organic moiety of
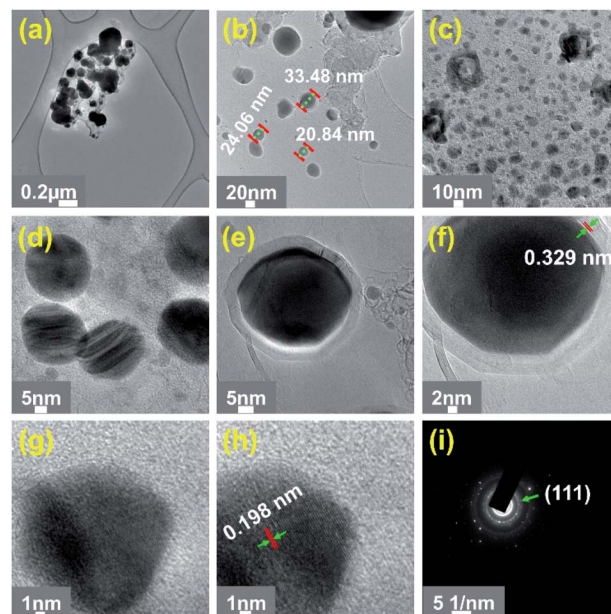
Fig. 2 (a–c) TEM micrographs with particle-size measurement of Co@NGr-900 (different resolution); (d–h) high resolution TEM images with lattice fringes measurement of Co@NGr-900; (i) SAED pattern of Co@NGr-900.

CoMOF-2 to N-doped carbon shells emerges at 900 °C. Probably, decay of the Cobalt MOF at low temperature carbonization releases metallic cobalt assisting the catalysis in the formation of carbon matrix as well as release of O_2 from the carboxylate and amide functional ligand moieties. The O_2 released from the ligand of CoMOF-2 can oxidize small amount of metallic cobalt to trivial amount of cobalt oxide (CoO_x), indeed reflected in XPS data of Co@NGr-900. As shown in Fig. 2a–d for Co@NGr-900, well-dispersed cobalt nanoparticles with varying sizes are encased by the carbon matrix. HR-TEM micrographs show that each cobalt nanoparticle is surrounded with few layers of N-doped graphitic shells (Fig. 2e–h).

The population of the cobalt nanoparticles generated at elevated temperature catalyze the graphitization process and assist the complete conversion of CoMOF-2 in the formation of N-doped graphitic shells. The graphitic shell imparts more stability and durability to Co@NGr-900 and proved to be very beneficial in protecting the cobalt nanoparticle from leaching out and often involve in electrocatalytic reactions. HR-TEM image was analyzed to determine the d-spacing in the case of Co@NGr-900. As depicted in Fig. 2h, the cobalt particles exhibit d-spacing of 0.198 nm between two adjacent lattice fringes corresponds to cubic cobalt plane of (111) and in the case of graphitic carbon (Fig. 2f) the d-spacing 0.329 nm matches to the (200) plane. Selected area electron diffraction (SAED) pattern exposed scattered diffraction spots from highly crystalline metallic cobalt endorsing the entrapment in the carbon shell (Fig. 2i). Detailed FE-SEM and TEM analysis not only revealed the progressive evolution but the crucial annealing temperature (900 °C) for the preparation of phase pure Co@NGr-900.
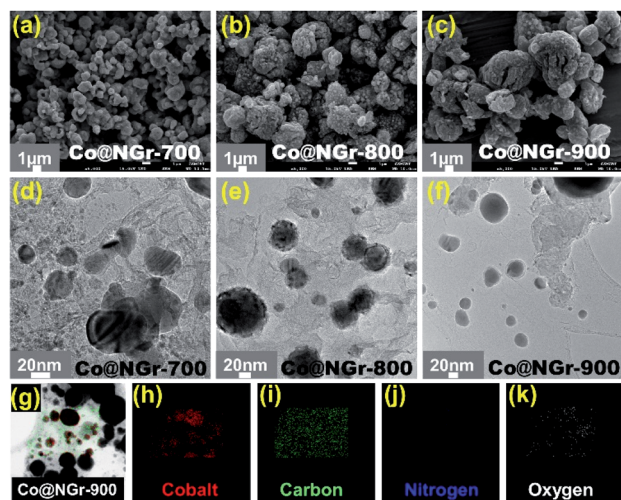

Fig. 1 (a–c) FE-SEM images of Co@NGr nanomaterials; (d–f) TEM images of Co@NGr nanomaterials; (g–k) STEM image/EDX elemental mapping of Co@NGr-900 nanomaterial.

The hybrid composite materials derived at different annealing temperatures were further investigated for their structural aspects and phase composition using PXRD data. Complete disappearance of the peaks from pristine CoMOF-2 and the presence of new peaks with identical pattern in all the three composite clearly demonstrate the formation of the nanostructured carbonized material. Powder X-ray diffraction (PXRD) patterns of Co@NGr-700, Co@NGr-800 and Co@NGr-900, JCPDS card for metallic cobalt and graphite for comparative analysis are provided in the Fig. 3a. Sharp peaks appeared at 44.3°, 51.6° and 75.9° from PXRD data for all the three samples can be assigned to metallic cobalt with crystalline facets of (111), (200) and (220) (JCPDS no. 00-015-0806). However, the reflections around 26.2° corresponding to (002) facet of the graphitic carbon (JCPDS no. 01-075-1621) seemed to be very weak in all the three samples reflecting the amorphous nature of the carbon shells. However, as shown in Fig. 3b zoomed version of the PXRD data shows a peak at around 26.2° for the (002) facet in all the three carbonized samples with an increase in peak intensity and sharpness for Co@NGr-900, clearly validating the formation of amorphous graphitic carbon shells. PXRD data clearly demonstrate entrapment of highly crystalline metallic cobalt in the carbon matrix.

Raman spectroscopy of all the three composite material was performed using Micro-Raman Spectroscopy system with 532 nm line of an Ar-ion laser at room temperature to evaluate the graphitization structure (Fig. 3c and S7†). All the samples showed three noticeable peaks, conforming D, G, 2D bands and the enhanced intensity as well as the sharpness of the peaks obviously establish the higher degree and complete graphitization at 900 °C. As depicted in Fig. 3c, typical D/G appeared at 1360/1592 cm^{-1} in the case of Co@NGr-900 and the sharp 2D band appeared at 2706 cm^{-1} can be attributed to the ultra-thin graphitic layers surrounding the metallic cobalt as observed in the HR-TEM analysis.[49] Conventionally D/G band corresponds

to disordered carbon and ordered sp^2-graphitic carbon respectively. Observed ID/IG value 0.85 for Co@NGr-900 discloses the carbon is well graphitized with an active distortion due to the N-doping and existence of metallic cobalt in the carbon matrix concurring with HR-TEM and PXRD results, favoring for accelerating ion transfer in improving electrochemical activity. XPS tests were performed to examine the surface chemistry and bonding configurations of Co@NGr composites. The full scan survey spectra exposed carbon, oxygen, nitrogen, and cobalt as possible elements are present in carbonized products (Fig. S8†). Table S1† provide the details of the atomic percentage of respective elements present in the carbonized material. Upon increasing the carbonization temperature except for carbon, atomic percentage for rest of the elements show a decreasing trend with only small amount of nitrogen (0.69%) existing in Co@NGr-900. Thus, complete carbonization process of the CoMOF-2 with mild doping of nitrogen in the carbon shells entrapping cobalt nanoparticles achieved at 900 °C in the formation of Co@NGr-900. Fig. 3d–f represents the high-resolution XPS spectra of Co 2p, C 1s, and N 1s regions respectively. The deconvoluted Co 2p spectrum showed two peaks at 780.8 eV (Co $2p_{3/2}$) and 796.7 eV (Co $2p_{1/2}$) (Fig. 3d). In addition, peaks at 785.6 eV, 796.7 eV suggest presence of a trivial amount of cobalt oxide and the 802.9 eV peak can be assigned as a satellite peak.[50] The C 1s spectrum is fitted by two peaks at 284.8 eV (C–C) and 285.7 eV (C=N) indicates the heteroatom doping in carbon matrix of the Co@NGr-900 and weak satellite peak appeared at 288.7 eV (Fig. 3e). The N 1s spectrum reveals peaks at 399.1 eV (pyridinic), 401.5 eV (pyrrolic) and 403.8 eV (graphitic nitrogen), inducing distortion in the carbon matrix playing an important role in electrocatalysis (Fig. 3f).[51] The pore-size and surface area analysis of Co@NGr-900 revealed micro/mesopores in the range of 0.6–0.7 nm and 3–9 nm, and specific surface area (54.9 m^2 g^{-1}) respectively (Fig. S9–S11 and Table S2†). Characterization by
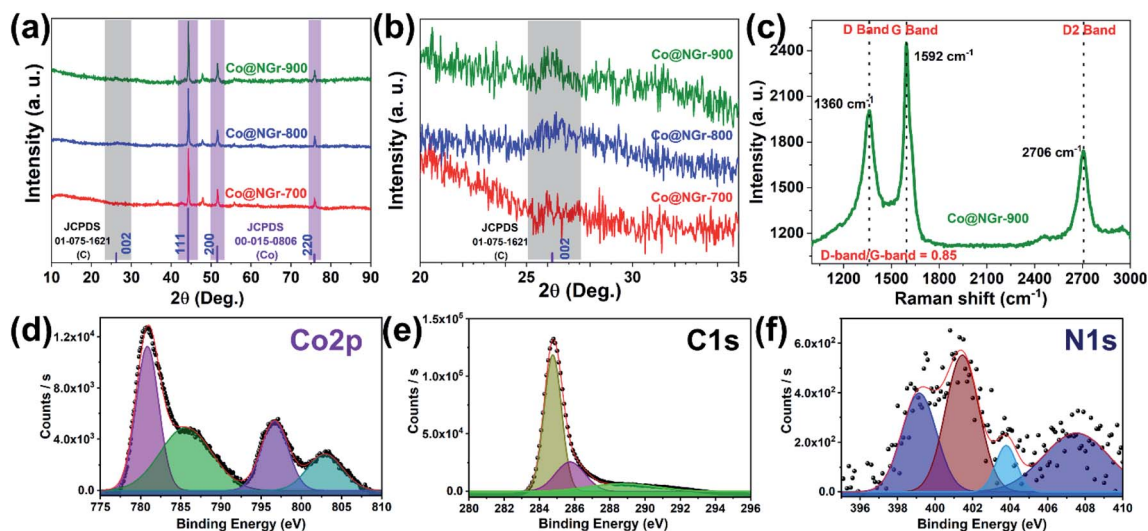

Fig. 3 (a and b) PXRD patterns of Co@NGr-700/800/900 nanomaterials compared with graphitic carbon and metallic cobalt JCPDS reference patterns; (c) FT-Raman spectrum of Co@NGr-900; (d–f) High resolution XPS spectrum of Co@NGr-900 for Co 2p, C 1s and N 1s.

versatile analytical method endorse the fabrication of Co-encapsulated heteroatom doped carbon composite, which believed to play vital role as an excellent electrocatalyst. The cobalt/nitrogen entrapment in the carbon matrix can assist the porosity, high surface area and electronic interaction of the composite is also beneficial for the mass transport favoring electrochemical activity of Co@NGr-900.

Electrochemical performance of Co@NGr

The unique nitrogen-doped carbon framework encased with cobalt nanoparticles endows large active surface area with homogeneous distribution of active nanoparticles within the nanosheets for improved mass transfer and conductivity can probably exhibit proficient electrocatalytic performance. Hence, we decided to explore the potential of the annealed CoMOF-2 derived carbon nanomaterials for its electrochemical performance based on the unique structural features and compositional advantages. Cyclic voltammetry (CV) and linear sweep voltammetry (LSV) have been implemented to evaluate the electrochemical properties of the calcined samples using a three-electrode electrochemical cell (ESI†). Electrocatalytic experiments were performed using respective materials loaded on glassy carbon electrode (GCE) devised as a working electrode, while Pt and Ag/AgCl electrode was used as counter and reference electrode respectively. All the activated calcined material was subjected to CV for 50 cycles (5 mV s^{-1}) to validate stability of catalyst and the OER performance was evaluated by iR-corrected linear sweep voltammetry (LSV) at scan rate of 5 mV s^{-1} in the 1 M KOH alkaline solution. The obtained polarization curve of calcined materials in LSV exhibits higher currents at lower potentials (Fig. 4a and b).

All the calcined Co@NGr material revealed good OER activity and Co@NGr-900 showed lower potential compared to other

samples. In particular, for Co@NGr-900 the observed potential at a current density of 10 mA cm^{-2} was 1.62 V ($vs.$ RHE) compared with 1.51 V for RuO$_2$. The electrocatalytic properties of each calcined materials were evaluated by comparing the overpotential at 10 mA cm^{-2} current density. The required potential and its corresponding overpotential to obtain 10 mA cm^{-2} current density for all the materials are measured (Fig. 4a) and tabulated in Table 1. Co@NGr-900 required overpotential of 390 mV to obtain standard current density of 10 mA cm^{-2}, significantly lower than 430 mV and 470 mV for Co@NGr-800 and Co@NGr-700 respectively. 10 mA cm^{-2} current density has been adopted as standard metric by OER literature as well as solar fuel synthesis and Co@NGr-900 attained this mark by an overpotential of 390 mV, which is on higher side compared to the benchmark RuO$_2$ (280 mV) but comparable with literature reports (Table S4†).[33] To obtain 50 mA cm^{-2} current density, overpotential of 520 mV is required for Co@NGr-900 nanocomposite and 590/700 mV in the case of Co@NGr-800 and Co@NGr-700 respectively (Fig. 4b and Table S3†).

OER trend for carbonized products were in the order Co@NGr-900 > Co@NGr-800 > Co@NGr-700 at 10 mA cm^{-2} as well as 50 mA cm^{-2}. Tafel slope was calculated from each anodic polarization curve of Co@NGr electrocatalyst to

Table 1 Summary of overpotential for OER and HER for different Co@NGr nanomaterials at ±10 mA cm^{-2}

Co@NGr nanomaterials	Overpotential (mV) for OER	Overpotential (mV) for HER
Co@NGr-700	470	779
Co@NGr-800	430	403
Co@NGr-900	**390**	**340**

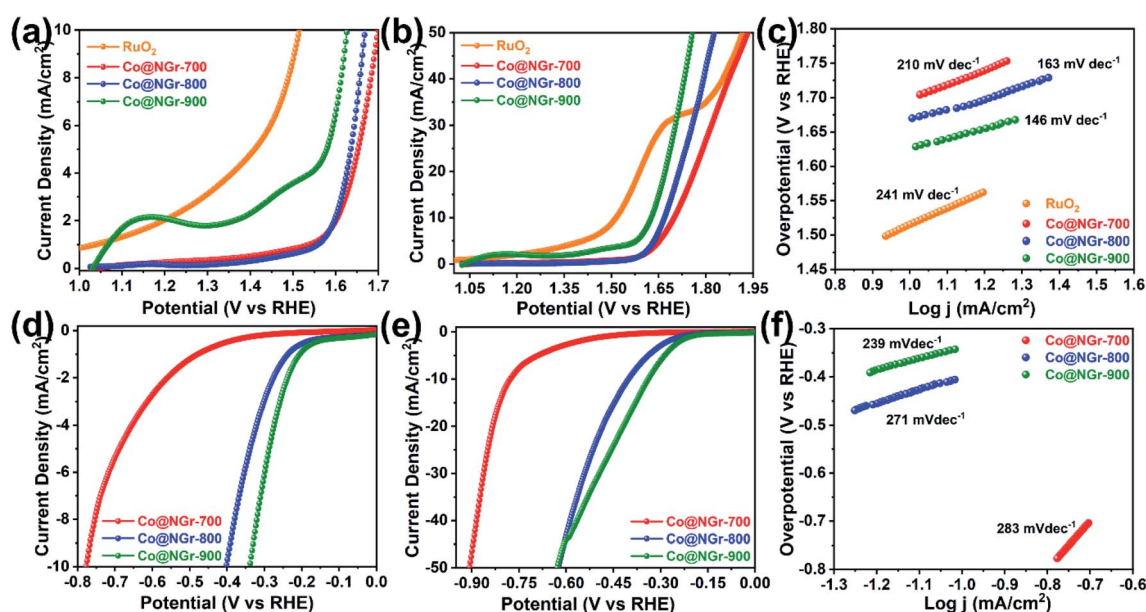**Fig. 4** (a–c) LSV plots and Tafel plots (OER) of Co@NGr-700/800/900 nanomaterials and RuO$_2$ at 10/50 mA cm^2; (d–f) LSV plots and Tafel plots (HER) of Co@NGr-700/800/900 nanomaterials at −10/−50 mA cm^{-2}.

determine the steady-state of the electrocatalytic material and shown in Fig. 4c. The resulting Tafel slop for Co@NGr-900 was 146 mV dec^{-1}, smaller than that of Co@NGr-800 and Co@NGr-700 (163 mV dec^{-1} and 210 mV dec^{-1}). The above data advocate the applicability of Co@NGr-900 catalyst for OER reaction delivering good catalytic performance.

The HER was performed using the composite materials in the H$_2$SO$_4$ solution (0.5 M) adopting a similar electrode system mentioned in OER analysis. The LSV curves were measured at scan rate of 5 mV s^{-1} and the corresponding plots are provided in the Fig. 4d and e. Linear sweep voltammetry (LSV) curves clearly disclose Co@NGr-900 material can achieve the current density of −10 mA cm^{-2} at an overpotential of 340 mV vs. RHE in acidic 0.5 M H$_2$SO$_4$ with superior catalytic performance with lower overpotentials compared to other carbonized materials. However, the observed overpotential for Co@NGr-700, and Co@NGr-800 to achieve −10 mA cm^{-2} current density being 403 and 779 mV respectively (Table 1 and Fig. 4d). The required overpotential to achieve −50 mA cm^{-2} current density is also given in the Fig. 4e and Table S3,† which follows the same trend of overpotential observed for −10 mA cm^{-2} current density. Thus, to obtain −50 mA cm^{-2} current density, an overpotential of 628 mV was required for Co@NGr-900 while 625/908 mV was observed in the case of Co@NGr-800 and Co@NGr-700 respectively. Albeit, these obtained results are not promising, but comparable with cobalt-entrapped carbon composite materials reported in the literature (Table S5†).[34] The relevant Tafel slope of the Co@NGr-900 catalyst (239 mV dec^{-1}) was also smaller than those of Co@NGr-800 (271 mV dec^{-1}) and Co@NGr-700 (283 mV dec^{-1}) exemplifying more beneficial electrocatalytic kinetics of the Co@NGr-900 catalyst for the HER (Fig. 4f).

Based on the literature, the probable electrocatalytic reaction mechanism for OER and HER is proposed as depicted in the Fig. 5.[52–54] The electrocatalyst adsorbs the reactant on its surface and form an intermediate in facilitating the electrocatalysis. The intermediate thus formed enables the charge transfer between an electrode and the reactant. In this work, the pyrolyzed cobalt-based MOF material was used as electrode material for electrochemical reactions. The OER and HER activities of pyrolyzed material were evaluated using a standard three-electrode electrochemical system in 1.0 M KOH and 0.5 M H$_2$SO$_4$ electrolytes. The OER is a four-step process, and 4

electrons need to be transferred for each O$_2$ molecule generation (Fig. 5a). In this process, OH$^-$ ion adsorbed on the active site of electrocatalyst (M*) and forms M*–OH via 1-electron oxidation followed by conversion of M*–OH into M*–O via deprotonation and electron removal. The generated M*–O will transform into M*–OOH after an OH$^-$ ion coupled with 1-electron oxidation and engendering O$_2$ molecule and initial active electrocatalyst. On the other hand, the HER process involves three steps to generate H$_2$ molecule in an acidic medium (Fig. 5b). Initially, hydrogen intermediates (H_{ads}) are formed via the charge-induced discharge of protons or water in the Volmer reaction. Then the generated hydrogen intermediate (H_{ads}) produces H$_2$ molecule as a product either by a combination of one proton with H_{ads} species (Heyrovsky reaction) or a combination of two H_{ads} species directly (Tafel reaction).

Good surface area and porosity observed in Co@NGr-900 also could elicit easier mass transportation in assisting superior activity of Co@NGr-900 for HER in acid media. Stability of Co@NGr-900 was evaluated by cyclic voltammetry in 1 M KOH solution. The iR-corrected LSV of freshly loaded Co@NGr-900 material was recorded, then cyclic voltammetry (CV) was performed for 200 cycles at 5 mV s^{-1} followed by LSV (Fig. S12†). The polarization curve with steady anodic potential clearly demonstrates the stability of the catalytic material even after 200 CV cycles. This is further reinforced by the comparison of the TEM images of the recovered Co@NGr-900 with the pristine sample (Fig. S13†). Electrochemical impedance spectroscopy (EIS) is used for investigating the fundamental behavior of an electrode material and the data can establish electron transfer rate.[55] In EIS, a typical Nyquist plot is constituted by two regions, a high frequency region represented by a semicircle corresponding to charge transfer resistance (R_{ct}) occurring at the electrode/electrolyte interface, and a low frequency region representing a vertical line along the slope gradually varying from 45° to 90° exemplified the diffusion of ions in the electrode material. The EIS measurement of Co@NGr was carried out in the frequency range from 50 kHz to 100 mHz with applying alternating current (AC) perturbation potential amplitude of 10 mV (without applying any potential). Nyquist plot of the electrode materials Co@NGr-700, Co@NGr-800 and Co@NGr-900 entail a depressed semicircle and straight line in the high/low frequency region respectively (Fig. 6c and S14†). Nyquist plots dominate by the linear region indicating that electron transfer occurring at the electrode surface is strongly influenced by a diffusion-limited process. The diffusion-limited process in lower frequency is represented by the Warburg impedance (Z_w), specifying an impedance is a consequence of the diffusion layer between electrode surface material and the solution. However, in the case of Co@NGr-900 material, the vertical line observed in lower frequency region of Nyquist plot is much shorter than of Co@NGr-800/700 and also has steeper slope (>45°) suggesting the capacitive behavior of Co@NGr-900 material. The linearity in low-frequency region with steeper slope for Co@NGr-900 unveils a lower diffusive resistance and probably ensuing higher electrolyte ion diffusion into the electrode material supporting the better water splitting performance amongst the carbonized materials. Electrochemically
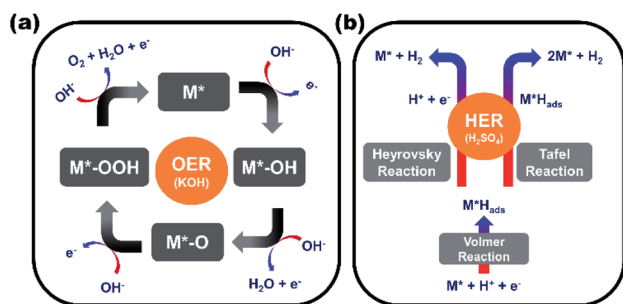

Fig. 5 Probable electrocatalytic mechanism for (a) oxygen evolution reaction (OER) and (b) hydrogen evolution reaction (HER) (M* = active site of electrocatalyst; H_{abs} = adsorbed hydrogen).
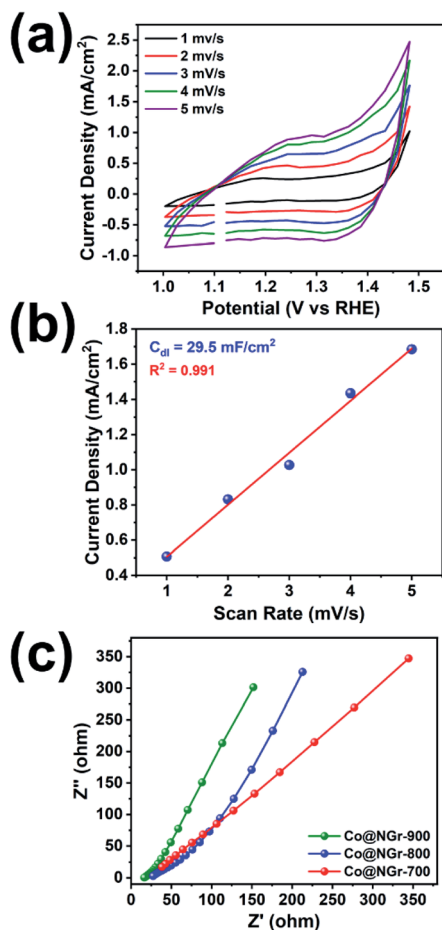
Fig. 6 (a) CV for Co@NGr-900 at different scan rates *vs.* RHE; (b) the linear fitting of current density at 1.43 V *vs.* RHE *vs.* different scan rates for Co@NGr-900; (c) Nyquist Plot for Co@NGr-700/800/900 nanomaterials.

range by operating cyclic voltammograms and the calculated EASA value found to be 737.5 cm^2. The electrocatalytic activity of Co@NGr-900 can be endorsed mainly to its composition *i.e.*, the presence of catalytically active cobalt as well as nitrogen-doped carbon matrix encasing the nano sized metal clusters. Uniform distribution of metallic cobalt can act as active centres promoting the oxidation of OH$^-$ into molecular oxygen in OER. Further, metallic nanoparticles can facilitate charge movements by improving surface wettability and electrical conductivity thereby enhancing the electrode–electrolyte interaction in the catalytic efficiency.[58–60] Furthermore, heteroatom doping in the form of nitrogen in the graphitic sheets, the nitrogen can interact with carbon creating C–N bonds, introducing disorder in the matrix as well as positive charge on the carbon atom. Electrostatic force between the positively charged carbon matrix can adsorb the OH$^-$ ion promoting the OER activity. In addition to this, the excellent electrical properties of N-doped graphene enhance the electrical conductivity of the Co@NGr-900 catalyst which further boosts the OER and HER performance by electron transfer. As observed in the case of Co@NGr-900 large surface area observed can provide sufficient ion-adsorption on the interface and the uniform distribution of active micro and mesoporous sites facilitate electrolyte ion-diffusion and provides more ion adsorption site for the efficient electrochemical process.

Conclusions

In summary, we could optimize the synthetic condition for the preparation of N-doped carbon-based cobalt-encapsulated electrocatalyst by carbonization of a cobalt based mixed ligand MOF showing good OER and HER performance. The spectroscopic and microstructural investigations of all the pyrolyzed product and the progression in the formation of Co@NGr-900 with N-doped graphitic carbon encasing metallic cobalt has been carefully analyzed. These nanomaterials were characterized by different analytical methods like PXRD, TEM, and XPS analyses and all the analytical methods exposed the uniform distribution of cobalt nanoparticles between thin layers of N-doped graphitic sheets in the case of Co@NGr-900. Optimized annealing temperature is crucial to get the phase pure bulk material Co@NGr-900 with the formation of cobalt nanoparticle and N-doping in the graphitic carbon material and, which provides active sites beneficial in OER and HER activities. The electrocatalytic properties of the obtained hybrid materials towards OER and HER were studied in 1 M KOH/0.5 M H$_2$SO$_4$ solution using various electrochemical techniques clearly demonstrate the good performance of Co@NGr-900 as bifunctional catalyst for water splitting. This work provides insight, practical and effective approach for preparing highly active and superior electrocatalyst towards next generation energy devices.

Author contributions

Dr Gopala Ram Bhadu and Dr Bhavesh Parmar: conceptualization, data curation, investigation, formal analysis,

active surface area is one of the main parameters attributable towards the essential properties of the electrocatalyst. Electrochemical double-layer capacitance (C_{dl}) is an important parameter to evaluate the active electrochemical surface area of catalysts in OER. High C_{dl} value reflects that the catalysts could expose more active sites to promote electrocatalytic oxygen generation. The double-layer capacitance (C_{dl}) is linearly proportional to the active surface area, which is established by the measurement of non-faradaic capacitive current.

The C_{dl} is directly proportional to effective active surface area (EASA) besides conductivity of the material and EASA of Co@NGr-900 was evaluated as per the reported literature.[41,56,57] CV was performed in 1 M KOH for the potential range 1.0 to 1.5 V *vs.* RHE at various scan rates to measure C_{dl} value. The current densities *vs.* scan speeds at 1.43 V *vs.* RHE were plotted for Co@NGr-900, based on the CV (Fig. 6a). The plot exhibits a linear relationship and the slope of this line reveals the C_{dl} of Co@NGr-900 catalyst (29.5 mF cm^{-2}) reflecting exposed active sites towards efficient electrocatalytic activity (Fig. 6b). Electrochemically active surface area of Co@NGr-900 has been evaluated by assessing C_{dl} in a non-faradaic capacitive current

methodology, visualization, writing – original draft. Mr Parth Patel: investigation, formal analysis. Mr Jayesh C. Chaudhari: formal analysis. Dr Eringathodi Suresh: funding acquisition, validation, writing – original draft, writing – review & editing, project administration, supervision.

Conflicts of interest

There are no conflicts to declare.

Acknowledgements

References

1 E. Dogan and F. Seker, The influence of real output, renewable and non-renewable energy, trade and financial development on carbon emissions in the top renewable energy countries, *Renewable Sustainable Energy Rev.*, 2016, **60**, 1074–1085.

2 S. Chu and A. Majumdar, Opportunities and challenges for a sustainable energy future, *Nature*, 2012, **488**, 294–303.

3 J. A. Turner, Sustainable Hydrogen Production, *Science*, 2004, **305**, 972–974.

4 J. Hu, C. Zhai and M. Zhu, Photo-responsive metal/semiconductor hybrid nanostructure: A promising electrocatalyst for solar light enhanced fuel cell reaction, *Chin. Chem. Lett.*, 2021, **32**, 1348–1358.

5 J. Shan, Y. Zheng, B. Shi, K. Davey and S.-Z. Qiao, Regulating Electrocatalysts *via* Surface and Interface Engineering for Acidic Water Electrooxidation, *ACS Energy Lett.*, 2019, **4**, 2719–2730.

6 C. Long, K. Wang, Y. Shi, Z. Yang, X. Zhang, Y. Zhang, J. Han, Y. Bao, L. Chang, S. Liu and Z. Tang, Tuning the electronic structure of PtRu bimetallic nanoparticles for promoting the hydrogen oxidation reaction in alkaline media, *Inorg. Chem. Front.*, 2019, **6**, 2900–2905.

7 I. Roger, M. A. Shipman and M. D. Symes, Earth-abundant catalysts for electrochemical and photoelectrochemical water splitting, *Nat. Rev. Chem.*, 2017, **1**, 0003.

8 Y. Yan, B. Y. Xia, B. Zhao and X. Wang, A review on noble-metal-free bifunctional heterogeneous catalysts for overall electrochemical water splitting, *J. Mater. Chem. A*, 2016, **4**, 17587–17603.

9 Z.-P. Wu, X. F. Lu, S.-Q. Zang and X. W. Lou, Non-Noble-Metal-Based Electrocatalysts toward the Oxygen Evolution Reaction, *Adv. Funct. Mater.*, 2020, **30**, 1910274.

10 N.-T. Suen, S.-F. Hung, Q. Quan, N. Zhang, Y.-J. Xu and H. M. Chen, Electrocatalysis for the oxygen evolution reaction: recent development and future perspectives, *Chem. Soc. Rev.*, 2017, **46**, 337–365.

11 R. Frydendal, E. A. Paoli, B. P. Knudsen, B. Wickman, P. Malacrida, I. E. L. Stephens and I. Chorkendorff, Benchmarking the Stability of Oxygen Evolution Reaction Catalysts: The Importance of Monitoring Mass Losses, *ChemElectroChem*, 2014, **1**, 2075–2081.

12 Y. Lee, J. Suntivich, K. J. May, E. E. Perry and Y. Shao-Horn, Synthesis and Activities of Rutile IrO_2 and RuO_2 Nanoparticles for Oxygen Evolution in Acid and Alkaline Solutions, *J. Phys. Chem. Lett.*, 2012, **3**, 399–404.

13 R. Kötz, H. J. Lewerenz and S. Stucki, XPS Studies of Oxygen Evolution on Ru and RuO_2 Anodes, *J. Electrochem. Soc.*, 1983, **130**, 825–829.

14 E. Antolini, Iridium As Catalyst and Cocatalyst for Oxygen Evolution/Reduction in Acidic Polymer Electrolyte Membrane Electrolyzers and Fuel Cells, *ACS Catal.*, 2014, **4**, 1426–1440.

15 M. Li, Y. Xiong, X. Liu, X. Bo, Y. Zhang, C. Han and L. Guo, Facile synthesis of electrospun MFe_2O_4 (M = Co, Ni, Cu, Mn) spinel nanofibers with excellent electrocatalytic properties for oxygen evolution and hydrogen peroxide reduction, *Nanoscale*, 2015, **7**, 8920–8930.

16 Z. Lu, H. Wang, D. Kong, K. Yan, P.-C. Hsu, G. Zheng, H. Yao, Z. Liang, X. Sun and Y. Cui, Electrochemical tuning of layered lithium transition metal oxides for improvement of oxygen evolution reaction, *Nat. Commun.*, 2014, **5**, 4345.

17 R. Subbaraman, D. Tripkovic, K.-C. Chang, D. Strmcnik, A. P. Paulikas, P. Hirunsit, M. Chan, J. Greeley, V. Stamenkovic and N. M. Markovic, Trends in activity for the water electrolyser reactions on $3d$M(Ni,Co,Fe,Mn) hydr(oxy)oxide catalysts, *Nat. Mater.*, 2012, **11**, 550–557.

18 J. Nai, Y. Lu, L. Yu, X. Wang and X. W. Lou, Formation of Ni-Fe Mixed Diselenide Nanocages as a Superior Oxygen Evolution Electrocatalyst, *Adv. Mater.*, 2017, **29**, 1703870.

19 J. Wang, Y. Gao, H. Kong, J. Kim, S. Choi, F. Ciucci, Y. Hao, S. Yang, Z. Shao and J. Lim, Non-precious-metal catalysts for alkaline water electrolysis: operando characterizations, theoretical calculations, and recent advances, *Chem. Soc. Rev.*, 2020, **49**, 9154–9196.

20 J. D. Blakemore, R. H. Crabtree and G. W. Brudvig, Molecular Catalysts for Water Oxidation, *Chem. Rev.*, 2015, **115**, 12974–13005.

21 J. Lee, O. K. Farha, J. Roberts, K. A. Scheidt, S. T. Nguyen and J. T. Hupp, Metal–organic framework materials as catalysts, *Chem. Soc. Rev.*, 2009, **38**, 1450–1459.

22 B. L. Chen, S. C. Xiang and G. D. Qian, Metal-Organic Frameworks with Functional Pores for Recognition of Small Molecules, *Acc. Chem. Res.*, 2010, **43**, 1115–1124.

23 Y. J. Cui, B. Li, H. J. He, W. Zhou, B. L. Chen and G. D. Qian, Metal-Organic Frameworks as Platforms for Functional Materials, *Acc. Chem. Res.*, 2016, **49**, 483–493.

24 X. Han, S. Yang and M. Schröder, Porous metal–organic frameworks as emerging sorbents for clean air, *Nat. Rev. Chem.*, 2019, **3**, 108–118.

25 M. Ding, R. W. Flaig, H.-L. Jiang and O. M. Yaghi, Carbon capture and conversion using metal–organic frameworks

and MOF-based materials, *Chem. Soc. Rev.*, 2019, **48**, 2783–2828.

26 Z. Li, J. Hu, Y. Xiao, Q. Zha, L. Zeng and M. Zhu, Surfactant assisted Cr-metal organic framework for the detection of bisphenol A in dust from E-waste recycling area, *Anal. Chim. Acta*, 2021, **1146**, 174–183.

27 Z. Li and M. Zhu, Detection of pollutants in water bodies: electrochemical detection or photo-electrochemical detection?, *Chem. Commun.*, 2020, **56**, 14541–14552.

28 M. Jahan, Z. Liu and K. P. Loh, A Graphene Oxide and Copper Centered Metal Organic Framework Composite as a Tri Functional Catalyst for HER, OER, and ORR, *Adv. Funct. Mater.*, 2013, **23**, 5363–5372.

29 K. Shen, X. Chen, J. Chen and Y. Li, Development of MOF-Derived Carbon-Based Nanomaterials for Efficient Catalysis, *ACS Catal.*, 2016, **6**, 5887–5903.

30 S. H. Liu, Z. Y. Wang, S. Zhou, F. J. Yu, M. Z. Yu, C. Y. Chiang, W. Z. Zhou, J. J. Zhao and J. S. Qiu, Metal-Organic-Framework-Derived Hybrid Carbon Nanocages as a Bifunctional Electrocatalyst for Oxygen Reduction and Evolution, *Adv. Mater.*, 2017, **29**, 1700874.

31 S. Dang, Q.-L. Zhu and Q. Xu, Nanomaterials derived from metal–organic frameworks, *Nat. Rev. Mater.*, 2018, **3**, 17075.

32 Q. Wang and D. Astruc, State of the Art and Prospects in Metal–Organic Framework (MOF)-Based and MOF-Derived Nanocatalysis, *Chem. Rev.*, 2020, **120**, 1438–1511.

33 J. Du, F. Li and L. Sun, Metal–organic frameworks and their derivatives as electrocatalysts for the oxygen evolution reaction, *Chem. Soc. Rev.*, 2021, **50**, 2663–2695.

34 B. Zhu, R. Zou and Q. Xu, Metal–Organic Framework Based Catalysts for Hydrogen Evolution, *Adv. Energy Mater.*, 2018, **8**, 1801193.

35 X. Zou, X. Huang, A. Goswami, R. Silva, B. R. Sathe, E. Mikmekova and T. Asefa, Cobalt-Embedded Nitrogen-Rich Carbon Nanotubes Efficiently Catalyze Hydrogen Evolution Reaction at All pH Values, *Angew. Chem., Int. Ed.*, 2014, **53**, 4372–4376.

36 H. X. Zhong, F. L. Meng, X. B. Zhang, J. M. Yan and Q. Jiang, Recent advances in metal-nitrogen-carbon catalysts for electrochemical water splitting, *Mater. Chem. Front.*, 2017, **1**, 2155–2173.

37 Y. Cao, S. Mao, M. Li, Y. Chen and Y. Wang, Metal/Porous Carbon Composites for Heterogeneous Catalysis: Old Catalysts with Improved Performance Promoted by N-Doping, *ACS Catal.*, 2017, **7**, 8090–8112.

38 M. Zhang, Q. Dai, H. Zheng, M. Chen and L. Dai, Novel MOF-Derived Co@N-C Bifunctional Catalysts for Highly Efficient Zn–Air Batteries and Water Splitting, *Adv. Mater.*, 2018, **30**, 1705431.

39 X. Li, J. Wei, Q. Li, S. Zheng, Y. Xu, P. Du, C. Chen, J. Zhao, H. Xue, Q. Xu and H. Pang, Nitrogen-Doped Cobalt Oxide Nanostructures Derived from Cobalt–Alanine Complexes for High-Performance Oxygen Evolution Reactions, *Adv. Funct. Mater.*, 2018, **28**, 1800886.

40 X. Wang, X. Huang, W. Gao, Y. Tang, P. Jiang, K. Lan, R. Yang, B. Wang and R. Li, Metal–organic framework derived CoTe2 encapsulated in nitrogen-doped carbon nanotube frameworks: a high-efficiency bifunctional electrocatalyst for overall water splitting, *J. Mater. Chem. A*, 2018, **6**, 3684–3691.

41 G. R. Bhadu, B. Parmar, P. Patel, A. Paul, J. C. Chaudhari, D. N. Srivastava and E. Suresh, Co@N-doped carbon nanomaterial derived by simple pyrolysis of mixed-ligand MOF as an active and stable oxygen evolution electrocatalyst, *Appl. Surf. Sci.*, 2020, **529**, 147081.

42 R. P. Jia, Z. Z. Gan, H. Huang and Z. M. Sheng, Controlled synthesis of mesoporous carbon with ultra-high N-doping structure from polymer precursor for efficient electrocatalysis of oxygen reduction, *Electrochim. Acta*, 2021, **368**, 137617.

43 P. Huang, J. Lei, Z. Sun and X. Hu, Fabrication of MOF-derived CuOx-C electrode for electrochemical degradation of ceftazidime from aqueous solution, *Chemosphere*, 2021, **268**, 129157.

44 W. Yaseen, N. Ullah, M. Xie, W. Wei, Y. Xu, M. Zahid, C. J. Oluigbo, B. A. Yusuf and J. Xie, Cobalt–Iron nanoparticles encapsulated in mesoporous carbon nanosheets: A one-pot synthesis of highly stable electrocatalysts for overall water splitting, *Int. J. Hydrogen Energy*, 2021, **46**, 5234–5249.

45 W. Liu, L.-M. Ning, S.-Q. Li, W.-X. Liu, Q. Zhang, J. Shao and J.-L. Tian, N-rich MOFs Derived N-doped Carbon Nanotubes Encapsulating Cobalt Nanoparticles as Efficient and Magnetic Recoverable Catalysts for Nitro Aromatics Reduction, *J. Alloys Compd.*, 2021, 158333.

46 X. Liu and L. Dai, Carbon-based metal-free catalysts, *Nat. Rev. Mater.*, 2016, **1**, 16064.

47 Z. Liang, R. Zhao, T. Qiu, R. Zou and Q. Xu, Metal-organic framework-derived materials for electrochemical energy applications, *EnergyChem*, 2019, **1**, 100001.

48 B. Parmar, P. Patel, R. S. Pillai, R. K. Tak, R. I. Kureshy, N. H. Khan and E. Suresh, Cycloaddition of CO₂ with an Epoxide-Bearing Oxindole Scaffold by a Metal–Organic Framework-Based Heterogeneous Catalyst under Ambient Conditions, *Inorg. Chem.*, 2019, **58**, 10084–10096.

49 L. Zhang, X. Wang, R. Wang and M. Hong, Structural evolution from metal−organic framework to hybrids of nitrogen doped porous carbon and carbon nanotubes for enhanced oxygen reduction activity, *Chem. Mater.*, 2015, **27**, 7610–7618.

50 B. Y. Xia, Y. Yan, N. Li, H. B. Wu, X. W. Lou and X. Wang, A metal–organic framework-derived bifunctional oxygen electrocatalyst, *Nat. Energy*, 2016, **1**, 15006.

51 A. Aijaz, J. Masa, C. Rosler, W. Xia, P. Weide, A. J. R. Botz, R. A. Fischer, W. Schuhmann and M. Muhler, Co@Co₃O₄ encapsulated in carbon nanotube-grafted nitrogen-doped carbon polyhedra as an advanced bifunctional oxygen electrode, *Angew. Chem., Int. Ed.*, 2016, **55**, 4087–4091.

52 W. Yang, Z. Wang, W. Zhang and S. Guo, Electronic-Structure Tuning of Water-Splitting Nanocatalysts, *Trends Chem.*, 2019, **1**, 259–271.

53 M. Cui, X. Ding, X. Huang, Z. Shen, T.-L. Lee, F. E. Oropeza, J. P. Hofmann, E. J. M. Hensen and K. H. L. Zhang, Ni³⁺-Induced Hole States Enhance the Oxygen Evolution

Reaction Activity of $Ni_xCo_{3-x}O_4$ Electrocatalysts, *Chem. Mater.*, 2019, **31**, 7618–7625.

54 P. Mondal, J. Satra, D. N. Srivastava, G. R. Bhadu and B. Adhikary, $Pd^{\delta+}$-Mediated Surface Engineering of AgMnO4 Nanorods as Advanced Bifunctional Electrocatalysts for Highly Efficient Water Electrolysis, *ACS Catal.*, 2021, **11**, 3687–3703.

55 D. Cao and D. Cheng, One-pot synthesis of copper–nickel sulfide nanowires for overall water splitting in alkaline media, *Chem. Commun.*, 2019, **55**, 8154–8157.

56 M. A. Lukowski, A. S. Daniel, F. Meng, A. Forticaux, L. Li and S. Jin, Enhanced Hydrogen Evolution Catalysis from Chemically Exfoliated Metallic MoS_2 Nanosheets, *J. Am. Chem. Soc.*, 2013, **135**, 10274–10277.

57 J. Xie, S. Li, X. Zhang, J. Zhang, R. Wang, H. Zhang, B. Pan and Y. Xie, Atomically-thin molybdenum nitride nanosheets with exposed active surface sites for efficient hydrogen evolution, *Chem. Sci.*, 2014, **5**, 4615–4620.

58 D. Mattia, M. P. Rossi, B. M. Kim, G. Korneva, H. H. Bau and Y. Gogotsi, Effect of Graphitization on the Wettability and Electrical Conductivity of CVD-Carbon Nanotubes and Films, *J. Phys. Chem. B*, 2006, **110**, 9850–9855.

59 D. Yu, K. Goh, H. Wang, L. Wei, W. Jiang, Q. Zhang, L. Dai and Y. Chen, Scalable synthesis of hierarchically structured carbon nanotube–graphene fibres for capacitive energy storage, *Nat. Nanotechnol.*, 2014, **9**, 555–562.

60 R. R. Salunkhe, Y. V. Kaneti, J. Kim, J. H. Kim and Y. Yamauchi, Nanoarchitectures for Metal–Organic Framework-Derived Nanoporous Carbons toward Supercapacitor Applications, *Acc. Chem. Res.*, 2016, **49**, 2796–2806.